H. Leitner [a], H. Clemens [a], S. Höring [b], N. Wanderka [b], J. Banhart [b], P. Staron [c], B. Jamnig [d]

[a] Department of Physical Metallurgy and Materials Testing, University of Leoben,

Leoben, Austria

[b] Hahn-Meitner-Institute Berlin, Berlin, Germany

[c] Institute for Materials Research, GKSS Research Center,

Geesthacht, Germany

[d] Materials Center Leoben, Leoben, Austria

CHARACTERISATION OF PRECIPITATES IN A STAINLESS MARAGING STEEL BY THREE-DIMENSIONAL ATOM PROBE AND SMALL-ANGLE NEUTRON SCATTERING

Two complementary techniques, namely three-dimensional atom probe and small-angle neutron scattering, were employed to study precipitation phenomena in a stainless maraging steel (Fe-12.3%Cr-8.9%Ni-0.6%Si-1%Mo-0.6%Al-0.8%Ti, wt.%) during ageing at 475°C. Atom probe investigations revealed the precipitation of a single Ni-rich phase exhibiting an average particle diameter of 2.5 nm after 12 h. After ageing for 100 h these precipitates had grown to an average size of 4 nm. In addition, needle- or plate-like Ni-rich precipitates larger than 15 nm were present. Their compositions differ mainly in the amount of Fe, Ni and Ti. Furthermore, Cr-rich precipitates were observed. The size ranges and the number densities of the precipitates match well with those observed by small-angle neutron scattering.

Keywords: Maraging steel; Precipitation; Small-angle neutron scattering; Three-dimensional atom probe

1. Introduction

The term *maraging* relates to ageing reactions in very low-carbon martensitic steels. Due to precipitation hardening 0.2% yield stress values of up to 2.4 GPa can be achieved. Maraging steels are characterised by high Ni contents. They exhibit higher levels of ductility and toughness when compared to conventional high-carbon martensitic grades of equivalent strength. When quenched from austenitic conditions, maraging steels form a soft but heavily dislocated martensite. In this condition they can be easily machined and, if required, cold worked. The high Ni content lowers the martensite start temperature, but on reheating the martensite a distinctive hysteresis occurs, so that austenite is not reformed until the steel is held between 500 and 600°C. At lower temperatures, i.e. 400 to 500°C, precipitation of homogeneously dispersed intermetallic phases takes places, accelerated by the influence of the high dislocation density on the diffusion of substitutional solute atoms. Due to the low carbon content, carbide precipitation is practically eliminated.

The class of Cr-containing stainless maraging steels exhibits an excellent combination of high strength and hardness, ductility and toughness, combined with good corrosion resistance. As a consequence they are used in many technological sectors where weight saving is of great

importance such as aerospace and military. Ease of heat treatment and dimensional stability make these steels also attractive for use in machinery and tooling [1].

In the past years, several studies were conducted on precipitation phenomena in stainless steels. It has been shown that strengthening of Cr-containing stainless maraging steels is caused by the precipitation of different intermetallic phases, which takes place during ageing at temperatures above 400°C. The type of phases and their precipitation behaviour critically depend on alloy composition and heat treatment. In the following, the results obtained on Cr-containing stainless maraging steels similar to that used in this work are briefly reviewed. Stiller et al. [2, 3] reported that in the alloy Sandvik 1RK91 (Fe-13.2%Cr-8.6%Ni-2.4%Mo-1.7%Cu, wt.%) two different types of precipitates were detected after short ageing times. One type consists of almost pure copper, whereas the second type shows a composition close to $Ni_3(Ti,Al)$. Recently, a combination of three-dimensional atom probe (3DAP), transmission electron microscopy (TEM) and energy-filtered TEM (EFTEM) has revealed that three types of precipitates (instead of two) are responsible for the precipitation strengthening in this maraging steel [4]. These are a nickel-rich precipitate of undefined crystal structure, a quasicrystalline precipitate of icosahedral symmetry (R') and an ordered nickel-rich phase of the type $L1_0$, termed L-phase.

Gemperle et al. [5] studied a model alloy (Fe-11.2%Cr-9.1%Ni-1.3%Mo-1.2%Al-1%Ti, at.%) with a composition close to the alloy used in the present investigation. These authors reported that Ni_3Ti and $Ti_6Si_7Ni_{16}$ (G-phase) precipitates are present after ageing in the temperature range of 420 to 570 °C. The identification of the G-phase was performed by electron diffraction studies on extraction replicas and a qualitative chemical composition was obtained by electron-energy-loss-spectrometry (EELS). Sha et al. [6] investigated an identical steel by means of an atom probe. After ageing at 520°C for 5 hours, Ni_3Ti and $Ti_6Si_7Ni_{16}$ particles are present in the martensitic matrix, which confirms the results obtained by Gemperle et al. [5]. Furthermore, the formation of reverted austenite was observed. Despite the high Cr-content, no Cr-rich precipitates were detected.

The present work is focused on the precipitation behaviour of a high Cr-alloyed stainless maraging steel during ageing at 475°C. In order to investigate the chemistry of matrix and precipitates as well as particle shape and size distribution two complementary techniques, namely 3DAP and small-angle neutron scattering (SANS), were employed. Contrary to 3DAP, SANS enables the investigation of relatively large sample volumes. Precipitate size distributions and their changes due to heat treatments can easily be obtained. However, for a complete evaluation of the SANS data the exact composition of matrix and particles must be known.

2. Experimental

The chemical composition of the maraging steel investigated is listed in Table 1. The composition of this model alloy is close to that investigated by Gemperle et al. [5] and Sha et al. [6]. It should be noted that all further compositions presented in this paper are given in atomic percent. The material was solution annealed at 1000°C for 1 h and subsequently cooled in air. Ageing was performed at 475°C for both 12 h and 100 h. X-ray diffraction conducted on a specimen aged for 100 h showed no evidence for the existence of reverted austenite.

In order to prepare field ion microscopy (FIM) tips for 3DAP investigations, small rods with a cross section of 0.2×0.2 mm^2 were cut. Then the tips were prepared in two steps: first by electropolishing of the small rods in a solution of 15% perchloric and 85% acetic acid, and second by applying micro-electropolishing using an electrolyte of 2% perchloric acid in

butoxyethanol. A three-dimensional atom probe supplied by CAMECA was used. The measurements were performed at a temperature of about 60 K with a pulse fraction, i.e. the fraction of pulse voltage to the standing tip voltage, of 0.2 in ultra-high vacuum ($<10^{-8}$ Pa).

SANS was employed to analyse the evolution of the size distribution of the precipitates during aging. Basics of the SANS technique can be found elsewhere [7]. SANS was carried out on samples with a diameter of 25 mm and a thickness of 1 mm. Selector-monochromated neutrons with a mean wavelength of $\lambda = 0.57$ nm and a wavelength spread of $\Delta\lambda/\lambda = 10\%$ were used. The neutron beam impinging on the 1 mm thick samples had a diameter of 8 mm. Thus, the analysed volume is approximately 50 mm^3. The samples were magnetized to saturation in a field of 2 T. Four different detector distances (1 m, 3 m, 9 m, and 21 m) were used together with appropriate collimations to cover scattering vectors q from 0.02 to 2.5 nm^{-1} ($q = 4\pi\sin(\theta)/\lambda$, where 2θ is the scattering angle). Scattered neutrons were recorded with a $50{\times}50$ cm^2 area detector using $128{\times}128$ pixels. Measured intensities were corrected for sample transmission, background intensity and detector response. Macroscopic differential scattering cross sections were obtained by calibration against a vanadium standard. The error in the absolute scale of the obtained volume fractions introduced by this calibration is approximately 5%.

3. Results and discussion

3.1. Atom probe analyses

A representative example for a three-dimensional reconstruction of the location of Ni, Al, Ti, and Si atoms within the analysed volume of $9{\times}9{\times}28$ nm^3 of a sample aged at 475°C for 12 h is shown in Fig. 1a. The reconstructed volume contains regions enriched in Ni, Al, Ti, and Si. These regions are spherical with an average diameter of about 2.7 nm. The number density of these regions within the analysed volume is about $8.3{\times}10^{24}$ m^{-3}. Using a cluster-search algorithm it is possible to reconstruct clusters or small precipitates inside the scanned volume. Such a reconstruction is illustrated in Figs. 1b-e. The agglomeration of Ni atoms is displayed in Fig. 1b. Here only atoms within regions in which the local Ni concentration exceeds 20% are shown, while the remaining Ni atoms outside such regions are omitted. Analogous representations for Al atoms (minimum concentration 6 at.%), Si atoms (4 at.%) and Ti atoms (4 at.%) are displayed in Figs. 1c-e. Micro-chemical information of this alloy is obtained from concentration depth profiles. Using the data shown in Fig. 1 depth profiles through the core of precipitates were calculated by arranging a box with a cross section of $1.0{\times}1.0$ nm^2 as indicated in Fig. 1. The concentration values of the elements were calculated for slices of 0.4 nm thickness with an average increment of 0.2 nm. The concentration profiles of the constituting elements are summarised in Fig. 2. The relatively large statistical error is also indicated in Fig. 2. For the elements Mo and Mn no significant variations of the concentration are visible. The distribution of these atoms in the matrix and in the clusters is more or less random. The interface between matrix and clusters is rather sharp. Its effective width is about 1 nm. The chemical compositions of clusters and matrix are shown in Table 2. The overall compositions of the as-quenched state (Table 1) and the state after ageing for 12 h (Table 2) are slightly different which might be due to local concentration variations being always present in technical steel grades. The average particle composition was estimated from 22 particles. From Table 2 it is tempting to speculate that after ageing for 12 h at 475°C the clusters exhibit a composition of (Ni,Fe)$_3$(Ti,Al,Cr,Si).

Fig. 3 shows a three-dimensional reconstruction of the positions of Al and Ti atoms within the analysed volume of $11{\times}11{\times}92$ nm^3 after ageing at 475°C for 100 h. Several atom clusters are identified. Some of them contain more than 20 at.% Cr as determined by means of the cluster-search algorithm. In addition to these particles, regions enriched in Ni, Al and Ti are also

visible. The small Ni-rich particles of about 4 nm in diameter are spherical and particles larger than 15 nm exhibit a needle- or plate-like morphology. However, due to the restricted analysed volume no precise information on their shape can be given. The chemical compositions of the matrix and the three different precipitates observed after ageing at 475°C for 100 h are summarised in Table 3. Obviously, the compositions of the clusters observed after 12 h ageing and the small precipitates occurring after 100 h ageing are nearly identical and will be called *type I*. These precipitates do not grow essentially, i.e. from 2.5-3 nm after 12 h to only about 4 nm after 100 h of ageing.

The larger Ni-rich precipitates are called *type II*, while the Cr-rich phase consisting mainly of Cr and Fe define *type III*. Significant differences can be observed between the chemical composition of the precipitates of *type I* and *II*. They differ mainly in their Ni, Fe and Si content. While the small *type I* precipitates contain 28.7 at.% Ni and 42.0 at.% Fe, the large *type II* precipitates contain more Ni and less Fe, i.e. 49.3 at.% Ni and only 23.4 at.% Fe. The content of Si in the clusters of *type I* decreases from 6.1 at.% to 1.5 at.% of *type II* precipitate.

According to the 3DAP results (Table 2), the composition of the *type I* Ni-rich precipitates is roughly $(Ni,Fe)_3(Ti,Al,Cr,Si)$, which might be a precursor of a $(Ni,Fe)_3(Ti,Al)$-type phase that had been found in this steel by other investigators [5, 6]. In a previous study based on EFTEM and SANS analyses [8], however, it has been assumed that this type of precipitate represents a so-called G-phase $(Ti_6Ni_{16}Si_7)$. The existence of the G-phase in a nearly identical steel was reported by several authors [5, 6]. In the current study the composition of the large Ni-rich precipitates, probably situated at grain or lath boundaries, also resembles more of a $(Ni,Fe)_3(Ti,Al)$-type phase than a G-phase.

The formation of the precipitates in such alloys is very sensitive to details of the chemical composition. Alloys of nearly the same composition in Fe, Cr and Ni but varying amounts of elements like Mo, Si, Al, and Cu can behave differently. For example, in alloy IRK91 (Fe-13.2%Cr-8.6%Ni-2.4%Mo-1.7%Cu, wt.%) Mo-rich particles and Cu clusters appear first after short ageing times at a temperature of 475°C [2, 3]. This alloy contains much more Mo and additionally Cu as compared to the alloy investigated. On the other hand our alloy contains much more Si than the IRK91 alloy. This might be the reason why the precipitate, which is formed first, is rich on Si. In a steel of similar composition the formation of Ni_3Ti and $Ti_6Ni_{16}Si_7$ precipitates were found [5, 6].

However, 3DAP does not give information about the type of precipitates. Forthcoming TEM investigations will be conducted to gain information on the crystal structure and nucleation sites of the two Ni-rich precipitates and the Cr-rich precipitate which is assumed to represent a σ-type phase.

3.2. Small-angle neutron scattering

The scattering curve of the as-quenched sample is flat at large scattering vectors q (Fig. 4), indicating that a good homogenisation had been achieved by the solution heat treatment. The origin of the constant scattering contribution is atomic incoherent scattering and Laue scattering due to a statistical distribution of atoms of different species in the matrix. The increase in the cross-section at small q is due to unknown larger structures that are not influenced by ageing at 475°C.

The scattering curves of the sample aged for 12 h at 475°C showed an interference maximum that is caused by a high particle number density (Fig. 4). For a treatment of interparticle interference the local monodisperse approximation as described by Pedersen [9] has been adopted. In this approximation, the SANS scattering cross-section of a dispersion of precipitate particles is described in the framework of the two-phase model [7] according to

$$\frac{d\Sigma}{d\Omega}(q) = (\Delta\eta)^2 \int_0^\infty n(R)V(R)^2 F(q,R)^2 S(q,R_{HS},f_{HS})dR, \tag{1}$$

where $d\Sigma/d\Omega$ is the macroscopic differential scattering cross-section, $\Delta\eta$ is the difference in the scattering length densities of particle and matrix, $n(R)dR$ is the number density of particles with sizes between R und $R+dR$, and $V(R)$ is the particle volume. Smearing of the scattering curves due to the finite resolution of the pin-hole instrument was neglected because in our particular case the influence is small. The particle form factor $F(q,R)$ for spherical particles is [e.g., 10]:

$$F(q,r) = 3\frac{\sin(qr) - qr\cos(qr)}{(qr)^3}. \tag{2}$$

$S(q, R_{HS}, f_{HS})$ is the structure factor of the monodisperse hard-sphere model describing the interparticle interference effect. It can be calculated within the Percus-Yevick approximation [e.g., 11]. R_{HS} is the hard-sphere radius of a particle with radius R that is given by $R_{HS} = C_{HS}R$, where C_{HS} is a constant. R_{HS} can be interpreted by assuming a depleted zone around the particle in which no other particles can grow. f_{HS} is the volume fraction of hard spheres and is related to the actual particle volume fraction by

$$f_{HS} = f \cdot \left(\frac{R_{HS}}{R}\right)^3 = f \cdot C_{HS}^3. \tag{3}$$

A good fit in the q-region of interest could be achieved by the use of a single lognormal function for the particle size distribution $n(R)$:

$$n(R) = \frac{n_0}{\sqrt{2\pi}(\beta/R_0)R} \cdot \exp\left(-\frac{(\ln(R/R_0))^2}{2(\beta/R_0)^2}\right), \tag{4}$$

where R_0 and β describe the position of the maximum and the width of the distribution, and n_0 is the number density of particles contained in the distribution. On the other hand, the use of a normal distribution did not lead to satisfactory results. The distribution of the volume fraction is $\varphi(R) = n(R)V(R) = n(R)(4/3)\pi R^3$. The total volume fraction of particles contained in the distribution is $f = \int_0^\infty \varphi(R)dR$. The parameters n_0, R_0, and β, together with the additional parameter C_{HS}, are determined by fitting a scattering curve calculated by equation (1) to a measured scattering curve by means of a least-squares procedure.

In case of ferromagnetic material there is a magnetic scattering contrast $\Delta\eta_{mag}$ in addition to the nuclear one $\Delta\eta_{nuc}$. The magnetic scattering cross-section depends on the angle α between the scattering vector and the magnetic field. The precipitates are assumed to be non-magnetic and thus are considered as magnetic holes in the ferromagnetic matrix. When the matrix is magnetized to saturation and the chemical size of the precipitates is the same as their magnetic size, $(\Delta\eta)^2$ in equation (1) can be replaced by [12]:

$$(\Delta\eta)^2 = (\Delta\eta_{nuc})^2 + (\Delta\eta_{mag})^2 \cdot \sin^2\alpha. \tag{5}$$

Thus, the nuclear-cross section is measured at $\alpha = 0$, while the sum of nuclear and magnetic cross-section is measured at $\alpha = \pi/2$. The magnetic cross-section can thus be calculated by subtracting the data at $\alpha = 0$ from the data at $\alpha = \pi/2$. Only the magnetic cross-section is used here for the analysis of the particle size distribution, because in the case of non-magnetic

precipitates only the magnetic scattering length density of the matrix must be known for obtaining the volume fraction of all non-magnetic particles.

The magnetic scattering length density of the ferromagnetic matrix (index m) is calculated as $\eta_{mag,m} = p_m/v_m = p_0\mu_m/v_m$ with the magnetic scattering length p_m ($p_0 = 2.70{\times}10^{-13}$ cm [12]) and the mean magnetic moment per atom μ_m. The latter was calculated from the Fe ($\mu_{Fe} = 2.24\mu_B$) and Ni ($\mu_{Ni} = 0.60\mu_B$) moments and the corresponding matrix concentrations. The precipitates are assumed to be non-magnetic, which means that $\eta_{mag,p} = 0$. The mean volume per atom was calculated by $v_m = <M>/(\rho N_A)$, where M is the mean atomic mass, ρ is the density, and N_A is Avogadro's number. Numerical values for the relevant quantities used for fitting the scattering curves are summarised in Table 4.

After ageing at 475°C for 12 h the scattering cross-section at larger q-values has increased due to the formation of precipitates (Fig. 4). For fitting the scattering curves, the constant cross-sections determined from the as-quenched state were added to the calculated scattering cross-sections of the aged condition. Here it was assumed that the contribution from Laue scattering does not change significantly during ageing. The fit of the magnetic cross-section yields the size distribution shown in Fig. 5. The mean radius of the distribution is 1.45 nm and the precipitate number density is $7.0{\times}10^{24}$ m^{-3}. Both results agree well with the results obtained by 3DAP analysis. The precipitate volume fraction derived from Fig. 5 amounts to 6.6%. The results from fitting of the experimental SANS curves are stated in Table 5.

The SANS results obtained from the samples aged at 475°C for 100 h (Fig. 4) reveal that the precipitates have grown to a mean radius of 2.43 nm (Fig. 5 and Table 5), which corresponds well to the size of the small *type-I* Ni-rich precipitates found in the 3DAP analysis. The volume fraction of 7.0% is approximately the same as after ageing for 12 h at 475°C while the precipitate number density decreased to $2.2{\times}10^{24}$ m^{-3}, indicating that coarsening has occurred. It is assumed that the larger precipitates, which were detected by means of 3DAP analysis, are not completely contained in the large-R part of the size distribution shown in Fig. 5. However, the small-q part of the scattering curves does not change significantly during ageing. Thus, it is concluded that the volume fraction of the large precipitates is small when compared to the 7.0% contained in the size distribution.

4. Summary

The study of the precipitation behaviour in a stainless maraging steel during ageing at 475°C by means of 3DAP and SANS can be summarised as follows:

- After ageing for 12 h *type-I* precipitates enriched in Ni, Al, Ti, and Si are present within the martensitic matrix. The precipitates show a spherical shape and their average diameter is about 2.7 nm. These precipitates might be precursors of $(Ni,Fe)_3(Ti,Al)$-type phases which are commonly found in this steel grade.

- An ageing time of 100 h leads to the presence of two different types of Ni-rich precipitates, which differ in composition and shape. The smaller *type-I* precipitates are still spherical with an average diameter of 4 nm. The larger ones show a needle or plate-like morphology with a long axis exceeding 15 nm. In addition, after 100 h at 475°C a Cr and Fe-rich phase (*type-III* precipitate) is observed.

- The size ranges of the small precipitates obtained by 3DAP agree well with the results derived from SANS investigations. The large precipitates fall outside the size range accessible to the current SANS measurement.

References

[1]   R. F. Decker, S. Floreen: R. K. Wilson (Ed.) Maraging Steels: Recent Developments and Applications, TMS, Warrendale, PA, USA (1988) 1-38.

[2]   K. Stiller, M. Hättestrand, F. Danoix: Acta Mater. 46 (1998) 6063.

[3]   K. Stiller, F. Danoix, M. Hättestrand: Mater. Sci. Eng. A 250 (1998) 22.

[4]   M. Hättestrand, J-O. Nilsson, K. Stiller, P. Liu, M. Andersson: Acta Mater. (2004) in press.

[5]   A. Gemperle, J. Gemperlova, W. Sha, G.D.W. Smith: Mater. Sci. Techn. 8 (1992) 546.

[6]   W. Sha, A. Cerezo, G.D.W. Smith: Metall. Trans. A 24A (1993) 1241.

[7]   G. Kostorz: G. Kostorz, H. Herman (Eds.) Treatise on Materials Science and Technology, Vol. 15: Neutron Scattering, Academic Press (1979).

[8]   P. Staron, B. Jamnig, H. Leitner, R. Ebner, H. Clemens: J. Appl. Cryst. 36 (2003) 415.

[9]   J.S. Pedersen: J. Appl. Cryst. 27 (1994) 595.

[10]   A. Guinier, G. Fournet: Small-Angle Scattering of X-Rays, John Wiley&Sons, Chapman & Hall (1955).

[11]   D.J. Kinning, E.L. Thomas: Macromolecules 17 (1984) 1712.

[12]   G.E. Bacon: Neutron Diffraction, Clarendon Press, Oxford (1975).

Tables

Table 1: Chemical analysis of the maraging steel investigated (as-quenched state).

	Fe	Cr	Ni	Si	Ti	Al	Mo	Mn	C
at.%	Bal.	13.03	8.34	1.08	0.95	1.16	0.56	0.11	0.05
wt.%	Bal.	12.3	8.89	0.55	0.83	0.57	0.98	0.11	0.01

Table 2: Chemical composition (in at.%) of matrix and precipitated particles after ageing at 475°C for 12 h.

	Fe	Cr	Ni	Si	Ti	Al	Mo	Mn	C
Matrix	75.2	8.2	10.4	1.4	1.1	1.4	1.7	0.5	0.1
Precip. **type I**	44.7±3.7	5.1±1.8	26.1±3.8	5.7±1.6	5.6±1.7	10.5±1.5	1.7±0.6	0.6±0.4	0

Table 3: Chemical composition (in at.%) of precipitates and matrix after ageing at 475°C for 100 h.

	Fe	Cr	Ni	Si	Ti	Al	Mo	Mn	C
Matrix	81.4±0.7	10.4±0.1	5.0±0.1	0.6±0.1	0.4±0.1	0.2±0.1	1.4±0.2	0.5±0.1	0.03
Small precip. **type I**	42.0±3.9	5.6±1.2	28.7±3.1	6.1±0.9	3.4±0.8	10.7±0.6	2.8±1.0	0.7±0.4	0.04
Large precip. **type II**	23.4±6.5	6.0±1.9	49.3±4.4	1.5±0.04	6.0±0.5	10.6±0.4	2.7±0.2	0.6±0.1	0.02
Cr precip. **type III**	46.5±1.7	40.9±2.7	7.3±3.5	0.9±0.1	0.8±0.4	0.6±0.5	2.6±0.1	0.5±0.2	0

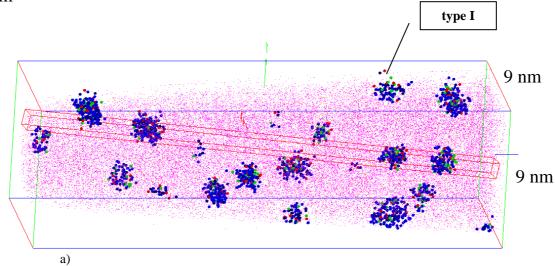Table 4: Data used for the analysis of small-angle neutron scattering curves.

	475°C/12 h	475°C/100 h
ρ [g cm^{-3}]	7.8±0.1	7.8±0.1
v_m [nm^3]	0.0118±0.0002	0.0119±0.0002
μ_m [μ_B]	1.75±0.02	1.85±0.02
$\eta_{mag,m}$ [10^{10} cm^{-2}]	3.97±0.05	4.19±0.06
$\eta_{mag,p}$ [10^{10} cm^{-2}]	0	0

Table 5: Fitting results obtained from the magnetic cross section.

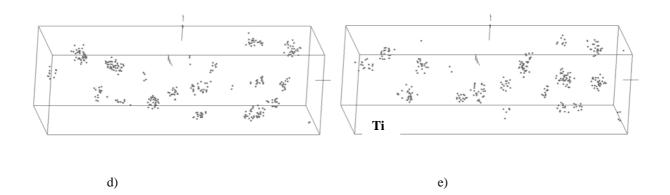| Sample	$\langle R \rangle$ [nm]	FWHM [nm]	n [10^{24} m^{-3}]	f [%]	C_{HS}
475°C/12 h	1.45	0.71	7.0± 0.4	6.6± 0.4	1.46±0.01
475°C/100 h	2.43	1.65	2.2±0.2	7.0±0.4	1.00±0.16

Figures

28 nm

Fig. 1: a) Three-dimensional reconstruction of the position of Ni, Al, Ti, and Si atoms in a volume of 9×9×28 nm^3 after ageing at 475°C for 12 h. Agglomeration of atoms in the same volume: b) Ni with a concentration above 20 at.%; c) Al with a concentration above 6 at.%; d) Si with a concentration above 4 at.%; e) Ti with a concentration above 4 at.%.
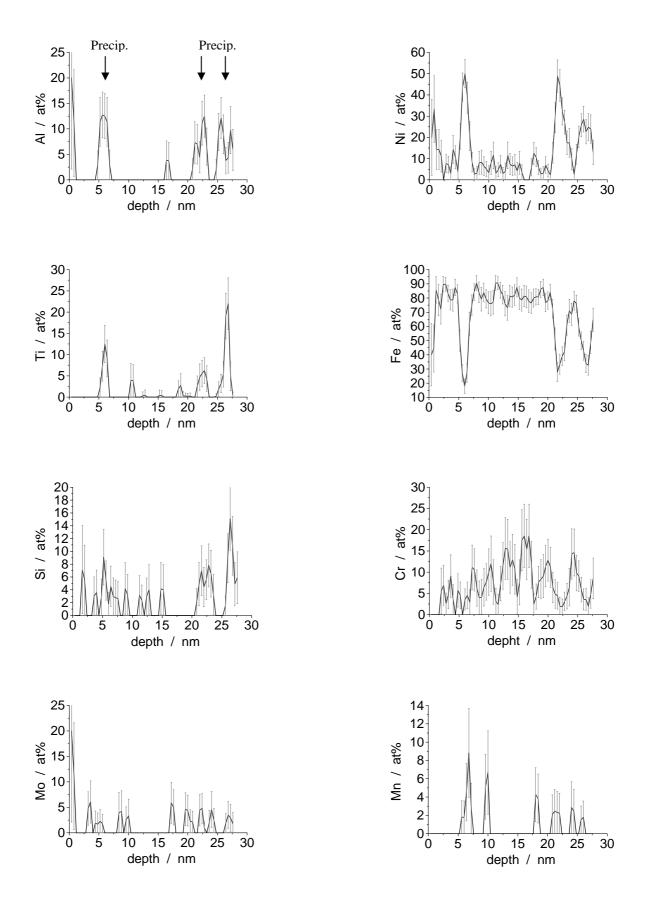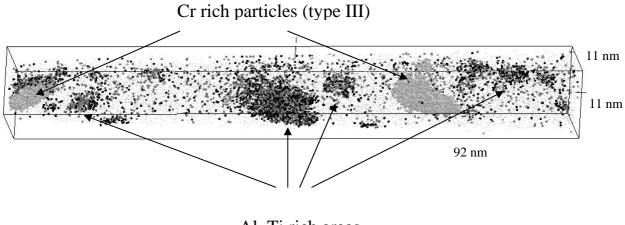
Fig. 2: Concentration depth profiles of the constituting elements (except C) after ageing at 475°C for 12 h. The analysed volume corresponds to the box indicated in Fig. 1a. The arrows denote the position of the analysed particles.

Fig. 3: Three dimensional elemental mapping of Al and Ti atoms within the analysed volume of $11 \times 11 \times 92$ nm^3. Chromium atoms within clusters with more than 20 at.% Cr concentration are displayed in the same volume.
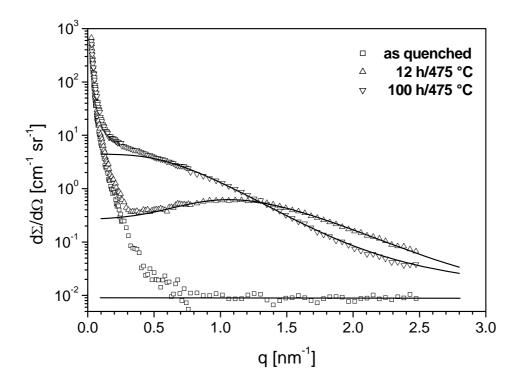

Fig. 4: Magnetic SANS cross-sections of an as-quenched sample and aged samples. Symbols: data; solid lines: fit.
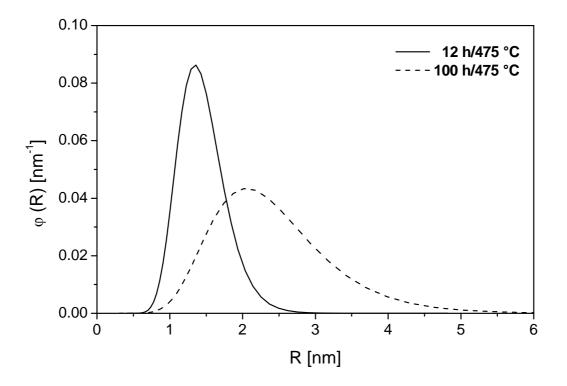
Fig. 5: Particle size distributions obtained from the magnetic SANS cross-section.